Fluid structure interaction simulations of aortic dissection

Richard Schussnig, Malte Rolf-Pissarczyk, Gerhard A. Holzapfel, Thomas-Peter Fries

Angaben zur Veröffentlichung / Publication details:

Schussnig, Richard, Malte Rolf-Pissarczyk, Gerhard A. Holzapfel, and Thomas-Peter Fries. 2021. "Fluid structure interaction simulations of aortic dissection." *PAMM* 20 (1): e202000125. https://doi.org/10.1002/pamm.202000125.

Received: 3 July 2020 | Accepted: 12 November 2020

DOI: 10.1002/pamm.202000125

Fluid-Structure Interaction Simulations of Aortic Dissection

Richard Schussnig[1,*], **Malte Rolf-Pissarczyk**[2], **Gerhard A. Holzapfel**[2,3], and **Thomas-Peter Fries**[1]

[1] Graz University of Technology, Institute of Structural Analysis, Lessingstraße 25/II,8010 Graz, Austria
[2] Graz University of Technology, Institute of Biomechanics, Stremayrgasse 16/II, 8010 Graz, Austria
[3] Norwegian University of Science and Technology, Department of Structural Engineering, 7491 Trondheim, Norway

The numerical modeling of aortic dissection (AD) is a particularly challenging biomechanical application, since the underlying coupling of tissue deformation and blood flow has to be considered, leading to a fluid-structure interaction (FSI) problem. To improve clinical relevance, patient-specific data and state-of-the-art constitutive models have to be incorporated. Computational methods to consider for tissue prestress and fiber orientation are presented herein.

1 Introduction

AD is a severe cardiovascular disease, featuring high mortality rates and requiring immediate surgical and/or medical treatment. This condition is characterized by the separation of aortic layers forming a so-called false lumen (FL), which allows the bloodstream to enter the tissue. Additionally, the fluid flow field in the newly created secondary volume is highly dependent on the position and geometry of the FL itself and possible tears in the intimal flap, which is the membrane between the true and the false lumen. Thus, the intimal flap is rather mobile, causing it to deform drastically during each cardiac cycle, while the outer wall portion is subject to comparably small deformations only [3]. With the fluid flow domain changing rapidly, also the forces acting on the solid vary vastly, resulting in a strongly coupled FSI problem. Several studies (see, e.g., [1–3]) came to the conclusion, that especially in the case of AD, the vessel compliance has to be accounted for, since disease progression and prognosis might be altered significantly.

2 Method

Reliable FSI simulations of AD require the combination of several modeling aspects which underlie clinical data. Based on the patient-specific geometric approximation and flow data taken from [3], the balance equations in the moving fluid domain $\Omega_\mathrm{f}(t)$, written in Arbitrary Lagrangian-Eulerian (ALE) form, are formulated as

$$\left.\begin{aligned} \rho_\mathrm{f}\hat{\partial}_t\boldsymbol{v} + \rho_\mathrm{f}(\boldsymbol{v}-\hat{\boldsymbol{v}})\cdot\nabla\boldsymbol{v} - \nabla\cdot\boldsymbol{\sigma}_\mathrm{f} &= \boldsymbol{0} \\ \nabla\cdot\boldsymbol{v} &= 0 \end{aligned}\right\} \text{ in } \Omega_\mathrm{f}(t), \quad \text{with} \quad \boldsymbol{\sigma}_\mathrm{f} = -p\boldsymbol{I} + \mu_\mathrm{f}\left[\nabla\boldsymbol{v} + (\nabla\boldsymbol{v})^\top\right]. \tag{1}$$

Therein, standard notations for the ALE time-derivative $\hat{\partial}_t(\cdot)$, domain velocity $\hat{\boldsymbol{v}}$ and fluid parameters given in Table 1 are adopted. Introducing the deformation gradient $\boldsymbol{F} = \boldsymbol{I} + \hat{\nabla}\hat{\boldsymbol{u}}$, the Jacobian $J = \det\boldsymbol{F}$ and the right Cauchy-Green tensor $\boldsymbol{C} = \boldsymbol{F}^\top\boldsymbol{F}$, the constitutive relation $\boldsymbol{S} = 2\partial\Psi/\partial\boldsymbol{C}$ is defined as [4]

$$\Psi = \frac{\mu_\mathrm{s}}{2}\left(\bar{I}_1 - 3\right) + \frac{\kappa_\mathrm{s}}{4}\left(J^2 - 1 - \ln J\right) + \frac{k_1}{2k_2}\sum_{i=4,6}\left[\exp\left\{k_2\left[\kappa\bar{I}_1 + (1-3\kappa)\bar{I}_i - 1\right]^2\right\} - 1\right], \tag{2}$$

using the invariants $\bar{I}_1 = J^{-2/3}\boldsymbol{C} : \boldsymbol{I}$ and $\bar{I}_i = J^{-2/3}\boldsymbol{C} : (\boldsymbol{M}_i \otimes \boldsymbol{M}_i)$, $i = 4, 6$, with symmetric mean fiber directions $[\boldsymbol{M}_i] = [\pm\sin\alpha, \cos\alpha, 0]^\top$. Then, the tissue displacement field $\hat{\boldsymbol{u}}$ is governed by the balance of linear momentum written as

$$\rho_\mathrm{s}\partial_{tt}\hat{\boldsymbol{u}} - \hat{\nabla}\cdot\left[\boldsymbol{F}\left(\boldsymbol{S}_0 + \boldsymbol{S}\right)\right] = \boldsymbol{0} \text{ in } \hat{\Omega}_\mathrm{s}, \tag{3}$$

where physiological parameters listed in Table 1 are used to capture the highly nonlinear and anisotropic material behavior of soft biological tissues – including the prestress $\boldsymbol{S}_0$ present in the reconstruction of the reference domain $\hat{\Omega}_\mathrm{s}$. The fluid and solid subproblems (1) and (3) are coupled on the fluid-structure interface $\Gamma_i(t) = \Omega_\mathrm{f}(t) \cup \Omega_\mathrm{s}(t)$ via

$$\boldsymbol{v} = \partial_t\hat{\boldsymbol{u}} \text{ on } \Gamma_i(t) \quad \text{and} \quad \hat{\boldsymbol{t}}_\mathrm{s} = \boldsymbol{F}\left(\boldsymbol{S}_0 + \boldsymbol{S}\right)\hat{\boldsymbol{n}}_\mathrm{s} = J\boldsymbol{\sigma}_\mathrm{f}\boldsymbol{F}^{-\top}\hat{\boldsymbol{n}}_\mathrm{s} = -\hat{\boldsymbol{t}}_\mathrm{f} \text{ on } \hat{\Gamma}_i, \tag{4}$$

applying a partitioned approach. Additionally, volumetric flow rates from [3] are prescribed on all in- and outlets. Exemplarily, the inlet mean velocity prescribed is depicted in Figure 1. On all the in- and outlets, the vessel wall is held fixed while the external tissue support is considered via the Robin condition enforced on the external boundary $\hat{\Gamma}_\mathrm{e}$

$$\hat{\boldsymbol{t}}_\mathrm{s} = -k_\mathrm{e}\hat{\boldsymbol{u}}_\mathrm{s} - c_\mathrm{e}\partial_t\hat{\boldsymbol{u}}_\mathrm{s} - p_\mathrm{e}\hat{\boldsymbol{n}}_\mathrm{s} \text{ on } \hat{\Gamma}_e \quad \text{with} \quad k_\mathrm{e} \approx 10^6\ \mathrm{N/m^3},\ c_\mathrm{e} \approx 10^7\ \mathrm{N/m^3 s} \quad \text{and} \quad p_\mathrm{e} = 7\cdot 10^3\ \mathrm{N/m^2}. \tag{5}$$

* Corresponding author: e-mail schussnig@tugraz.at, phone +43 316 873 6183, fax +43 316 873 106180

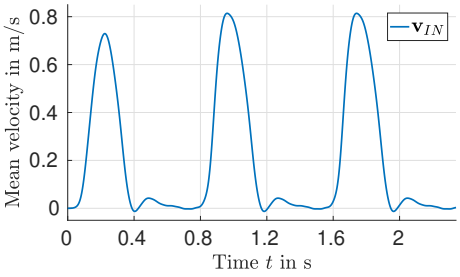

Fig. 1: Inlet velocity taken from [3].

Table 1: Physiological model parameters chosen.

Fluid density	ρ_f	1060 kg/m^3	Mean fiber direction	α	27.47 °
Dynamic viscosity	μ_f	0.004 Pa s	Dispersion parameter	κ	0.046
Solid density	ρ_s	1200 kg/m^3	Fiber parameter	k_1	121.98 kPa
Shear modulus	μ_s	150 kPa	Fiber parameter	k_2	5.01
Bulk modulus	κ_s	200 kPa			

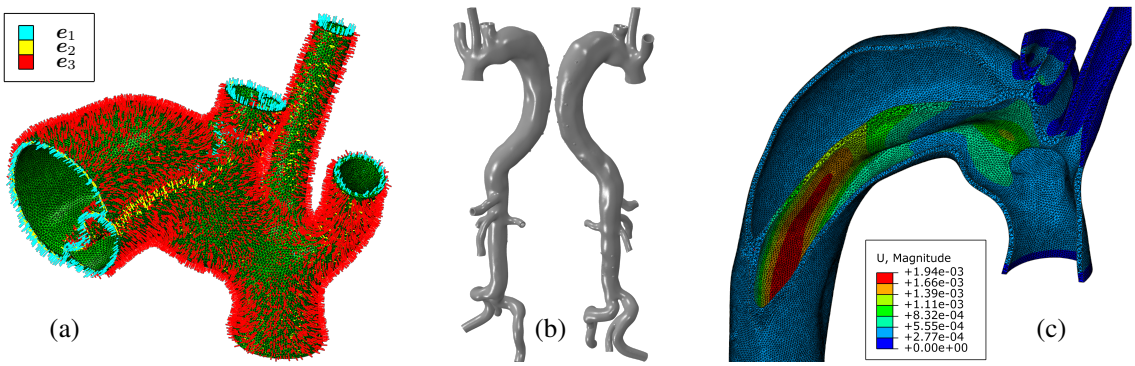

Fig. 2: Local coordinate system (a), computational domain (b) and deformation in cut arch region at $t = 2.05$ s (c).

The prestress $\boldsymbol{S}_0$ is computed using a slightly modified version of the algorithm proposed in [5] – introducing the shorthand notation $(\cdot)^k = (\cdot)(\boldsymbol{u}^k)$ for quantities depending on some displacement field $\boldsymbol{u}_k$, set $\boldsymbol{u}_0 = \boldsymbol{0}$ and iterate for $k > 1$ on static equilibrium including the known prestress $\boldsymbol{S}^{k-1}$, i.e.

$$-\hat{\nabla} \cdot \left[\boldsymbol{F}^k \left(\boldsymbol{S}^{k-1} + \boldsymbol{S}^k\right)\right] = \boldsymbol{0} \text{ in } \hat{\Omega}_\mathrm{s}, \quad \text{and} \quad \hat{\boldsymbol{t}}_\mathrm{s}^k = -\hat{\boldsymbol{t}}_\mathrm{f} \text{ on } \hat{\Gamma}_i \tag{6}$$

until $\|\boldsymbol{u}^k\| \approx 0$ with the fluid traction $\hat{\boldsymbol{t}}_\mathrm{f}$ obtained from a flow simulation with diastolic fluid boundary conditions and fixed, i.e., undeforming solid domain. Then, we set $\boldsymbol{S}_0 = \boldsymbol{S}^k$, which consequently results in $\hat{\boldsymbol{u}} \approx \boldsymbol{0}$ under diastolic flow conditions.

To construct a local coordinate system following the complex geometry, the unit-outward normal $\hat{\boldsymbol{n}}_s$ is extrapolated into the solid domain and taken in the circumferential direction $\boldsymbol{e}_3$. Solving for the scalar φ we have

$$-\hat{\nabla} \cdot \hat{\nabla}\varphi = 0 \text{ in } \hat{\Omega}_\mathrm{s} \quad \text{with} \quad \hat{\boldsymbol{n}} \cdot \hat{\nabla}\varphi = 0 \text{ on } \hat{\Gamma}_\mathrm{e} \quad \text{and} \quad \varphi = \varphi_D \text{ on } \partial\hat{\Omega}_\mathrm{s} \setminus \hat{\Gamma}_\mathrm{e}, \tag{7}$$

with boundary data φ_D set per outlet and the flux $\boldsymbol{q} = \hat{\nabla}\varphi$ approximates the fiber direction. To obtain $\boldsymbol{e}_1$ orthogonal to $\boldsymbol{e}_3$, rotate $\boldsymbol{q}$ in the plane spanned by $\boldsymbol{q}$ and $\boldsymbol{e}_3$ and complete the basis with normalized $\boldsymbol{e}_2$ orthogonal to $\boldsymbol{e}_1$ and $\boldsymbol{e}_3$.

3 Results and Conclusion

The local coordinate systems obtained are presented in Fig. 2(a), showing satisfactory behavior even in the flap region when considering symmetric fiber orientations. Incorporating the prestress $\boldsymbol{S}_0$ has a major effect on the stresses in and around the flap region. Nonetheless, displacements up to 1.94 mm are observed (Fig. 2(c)), while measurements of 8.7 mm were reported *in vivo* [3]. Thus, it becomes apparent that adapted parameters resembling diseased instead of healthy tissues have to be employed in future studies.

Acknowledgements The authors gratefully acknowledge Graz University of Technology for the financial support of the Lead-project *Mechanics, Modeling and Simulation of Aortic Dissection*.

References

[1] M. Alimohammadi, J. M. Sherwood, M. Karimpour, O. Agu, S. Balabani, and V. Díaz-Zuccarini, Biomed Eng Online **14**, 34 (2015).
[2] Y. Qiao, Y. Zeng, Y. Ding, J. Fan, K. Luo, and T. Zhu, Comput Methods Biomech Biomed Engin **22**, 620-630 (2019).
[3] K. Bäumler, V. Vedula, A. M. Sailer, J. Seo, P. Chiu, G. Mistelbauer, F. P. Chan, M. P. Fischbein, A. L. Marsden, and D. Fleischmann, Biomech Model Mechanobiol, in press.
[4] T. C. Gasser, R. W. Ogden, and G. A. Holzapfel, J R Soc Interface **3**, 15-35 (2006).
[5] M.-C. Hsu, and Y. Bazilevs, Finite Elem Anal Des **47**, 593-599 (2011).

